



Article

# Electrochemical Testing of Carbon Materials as Bromine Electrodes for the Hydrogen-Bromine Redox Flow Battery

Yaksh Popat <sup>1</sup>, David P. Trudgeon <sup>1</sup>, Xiaohong Li <sup>1,\*</sup>, Peter Connor <sup>1</sup>, Arunchander Asokan <sup>2</sup> and Matthew E. Suss <sup>2</sup><sup>1</sup> Renewable Energy Group, College of Engineering, Mathematics and Physical Sciences, University of Exeter, Penryn Campus, Cornwall TR10 9FE, UK<sup>2</sup> Faculty of Mechanical Engineering, Technion–Israel Institute of Technology, Haifa 3200003, Israel

\* Correspondence: x.li@exeter.ac.uk

**Abstract:** Hydrogen-bromine ( $H_2$ - $Br_2$ ) redox flow batteries (RFBs) have gained a lot of interest due to their advantages in mitigating the performance shortcomings of conventional zinc-bromine and vanadium flow batteries. Various carbon materials have been tested in  $H_2$ - $Br_2$  RFBs as bromine electrodes. However, a comparative study among the different carbon materials has not been reported in the literature. This work reports, for the first time, an evaluation of carbon papers, felt and cloth in a three-electrode half-cell setup as potential bromine electrodes, in pristine and thermally treated state. A systematic evaluation was performed by comparing the surface morphologies, kinetic parameters, polarisation curves and stability tests of different carbon electrodes. Thermally treated graphite felt electrode demonstrated the best electrochemical performance as bromine electrode owing to its improved surface area, hydrophilicity and intrinsic activity. Further in-depth studies will shed important insights, which will help understand the electrode characteristics for future bromine battery design. The current study will assist in evaluating the performance of upcoming novel electrode materials in a three-electrode assembly.



**Citation:** Popat, Y.; Trudgeon, D.P.; Li, X.; Connor, P.; Asokan, A.; Suss, M.E. Electrochemical Testing of Carbon Materials as Bromine Electrodes for the Hydrogen-Bromine Redox Flow Battery. *Batteries* **2022**, *8*, 166. <https://doi.org/10.3390/batteries8100166>

Academic Editor: Byunghoon Kim

Received: 24 August 2022

Accepted: 3 October 2022

Published: 7 October 2022

**Publisher's Note:** MDPI stays neutral with regard to jurisdictional claims in published maps and institutional affiliations.



**Copyright:** © 2022 by the authors. Licensee MDPI, Basel, Switzerland. This article is an open access article distributed under the terms and conditions of the Creative Commons Attribution (CC BY) license (<https://creativecommons.org/licenses/by/4.0/>).

**Keywords:** bromine electrode; carbon material; three-electrode setup; hydrogen-bromine; flow battery

## 1. Introduction

Industrial activities and population growth have resulted in a gigantic increase in the global energy demands and consumption. World energy production amounted to 617 EJ in 2019, and fossil fuels accounted for more than 81% of the production [1]. The combustion of fossil fuels is known to cause serious damage to the environment and the ecosystem due to the pollution. Over the past two decades, the contribution of renewables to the generation of electricity has increased, and the share of renewables in global electricity generation jumped to 29% in 2020 [2]. However, renewable energy sources, such as solar and wind, face some major challenges, such as high upfront cost, unpredictability, intermittency, geographical limitations, etc. Thus, energy storage is essential to tackle the uncontrollable and variable nature of renewable energy.

Redox flow batteries (RFBs) have been identified as one of the promising technologies for electrical energy storage (EES) because of their high efficiency, fast response, long cycle life, safe operation and environmental friendliness [3–5]. However, it is imperative that the electrolyte and the electrode materials used in an RFB are economical and abundant to ensure the energy storage system is sustainable and economically feasible. The hydrogen-bromine ( $H_2$ - $Br_2$ ) RFB meets these criteria owing to the abundance of hydrogen, bromine [6] and the cheap, scalable, carbon-based electrode materials used for the bromine electrode.  $H_2$ - $Br_2$  RFB is a promising candidate due to its advantages of: (a) high achievable energy density of the electrolyte; (b) good stability without significant degradation; (c) fast electrochemical reaction kinetics of hydrogen and bromine electrodes; (d) ability to undergo shallow discharges along with overcharge; and (e) high coulombic efficiency due to low self-discharge rate [7–9].

The corrosive nature of bromine restricts the choice of electrode materials to those that are corrosion resistant, durable and cheap, with high electrochemical performance for  $\text{Br}_2/\text{Br}^-$  redox reactions. Noble metal platinum shows excellent electrochemical activity for bromine redox reactions; however, it is expensive and unstable in HBr electrolytes, thereby hampering its use as an electrode material [10,11]. On the other hand, carbon materials have been reported as the most widely used electrode materials in bromine environments due to their advantages of low cost, excellent electrical conductivity and high corrosion resistance [12,13]. A carbon electrode with flexible design, yielding high mass loading, has been developed for supercapacitors [14]. Carbon felt, graphite felt and carbon paper are the three most widely used carbon electrode materials in bromine-based batteries [15–20]. Different 2D nanosheets (plates) on carbon cloth substrates have been demonstrated as electrodes for energy storage devices, such as supercapacitors and pseudocapacitors with high energy density [21,22]. Three-dimensional (3D) graphite felt is made from two kinds of precursors, namely polyacrylonitrile (PAN) and rayon (regenerated cellulose), by the process of needle punching, subsequently followed by graphitisation at 2000–2600 °C [23]. Carbon paper, composed of a cluster of crisscrossing carbon fibres with pores in the fibres [24], is typically much thinner (100–400 µm) than the graphite felt (2.5–10 mm). On the other hand, carbon cloth is a highly conductive textile, with a 3D network, which is made by weaving the carbon fibre, and it has a relatively more ordered fibre arrangement pattern and a broad pore distribution from 5 to 100 µm [25]. Carbon paper is non-woven, while carbon cloth is woven fabric; thus, no binder is normally needed for carbon cloth. Biomass-derived carbon materials have garnered a lot of interest recently owing to the sustainability, environmental friendliness, low cost and easy processing methods [26,27]. However, their application to bromine-based flow batteries has still not been explored.

While a comparison of carbon papers and felts has been previously reported in zinc-bromine and polysulfide-bromine systems, many reports emphasise carbon electrode materials, membrane influence and design optimisation in a full-cell RFB configuration [16,17,20,28]. The three-electrode configuration is vital in understanding the behaviour of different carbon materials in bromine environments by studying their reaction kinetics and surface properties. In this work, we report electrochemical studies and evaluation of carbon materials as bromine electrodes in a three-electrode half-cell setup. The materials were thermally treated to improve their activity for  $\text{Br}_2/\text{Br}^-$  redox reactions. The surface morphologies of the pristine and the heat-treated electrode materials were characterised by scanning electron microscopy and X-ray photoelectron spectroscopy. Linear sweep voltammetry, polarisation measurements and cycling tests were conducted to gain insights on the kinetic parameters, charge–discharge behaviour and stability of the different carbon electrode materials. This work provides a solid basis for designing future carbon-based bromine batteries by not only understanding their morphological influence but also their intrinsic catalytic activity for bromine reactions. Our current study can help benchmark the upcoming electrode materials in a three-electrode setup before validating them in an actual redox flow cell.

## 2. Experimental Section

### 2.1. Electrolyte Chemicals

Hydrobromic acid (ACS, 47–49%) and bromine (ACS reagent, >99.5%) were purchased from Alfa Aesar (Haverhill, MA, USA) and Sigma Aldrich (St. Louis, MO, USA), respectively. To investigate the electrode performance, 25 mL of 3 M HBr/1 M  $\text{Br}_2$  was used as the standard electrolyte for electrochemical experimentation. For the determination of electrode capacitance using cyclic voltammetry, 40 mL of 1 M KCl solution was used (Sigma Aldrich, St. Louis, MO, USA, 99.5%). All chemicals were used as received.

### 2.2. Electrode Materials and Setup

Six carbon materials were evaluated and reported as bromine electrodes in this work. Details of the materials are provided in Table 1. The carbon materials were used as received, without any modification. The carbon papers SGL 22AA and SGL 36AA were obtained from SGL Carbon (Wiesbaden, Germany), while the rest of the carbon materials (SGL

28AA, AvCarb MGL370, graphite felt (SGL, 2.5 mm) and ELAT Hydrophilic (carbon cloth)) were procured from Fuel Cell Store (College Station, TX, USA). The carbon materials were tested in a three-electrode half-cell setup consisting of the carbon material as the working electrode, Ag/AgCl reference electrode and graphite rod counter electrode (Figure 1). The electrochemical cell and the reference electrode were purchased from Pine Research instrumentation (USA), while the graphite rod (10 mm dia., 99.997%) was bought from Alfa Aesar. The carbon electrode substrate was prepared using a graphite-polymer composite (Eisenhuth, Osterode am Harz, Germany, BMA5 graphite/PVDF). The carbon material was cut and masked on the substrate with a PTFE tape (0.10 mm, RS components) to yield an effective exposed area of  $0.1\text{ cm}^2$ . The compression rate of the working electrode materials is essentially zero using this mounting technique. Each carbon material was tested in two different conditions—pristine and thermally treated. The thermal treatment was undertaken in a furnace by annealing the sample in air at  $550\text{ }^\circ\text{C}$  for 5 h with a heating rate of  $10\text{ }^\circ\text{C min}^{-1}$  (named as AN550 hereafter).

**Table 1.** Electrode materials under investigation.

Electrode Material	Manufacturer	Type	Porosity (%)	Thickness
22AA	SGL Carbon	Carbon paper	90	$120\text{ }\mu\text{m}$
28AA	SGL Carbon	Carbon paper	82	$190\text{ }\mu\text{m}$
36AA	SGL Carbon	Carbon paper	90	$185\text{ }\mu\text{m}$
MGL370	AvCarb	Moulded graphite laminate	78	$370\text{ }\mu\text{m}$
ELAT Hydrophilic Cloth	Nuvant Systems	Woven carbon cloth	80	$406\text{ }\mu\text{m}$
GFD Graphite Felt	SGL Carbon	Graphite felt	94	2.5 mm

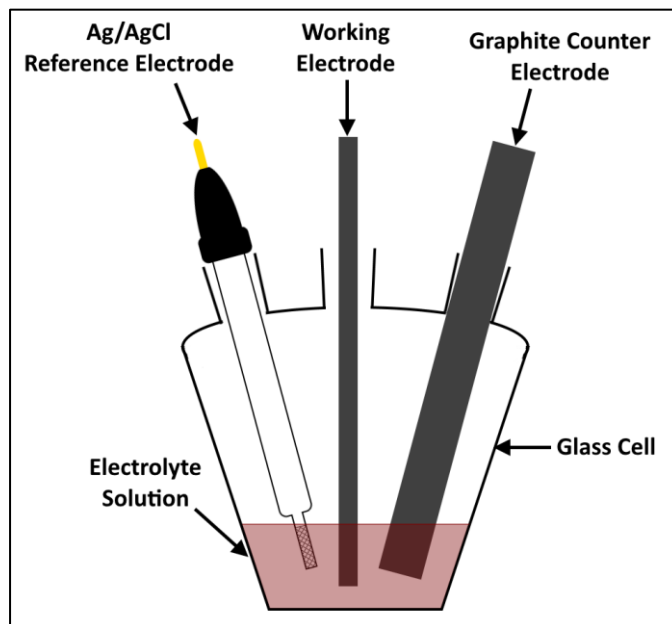


**Figure 1.** Schematic of the three-electrode half-cell setup.

### 2.3. SEM and XPS Characterisation

The surface morphologies of the samples were characterised using a FEI Quanta FEG 650 scanning electron microscopy (SEM), operated at an accelerating voltage of 5 kV and a working distance of 14 mm. The X-ray photoelectron spectroscopy (XPS) was recorded using a Thermo VG Scientific Sigma Probe system (Waltham, MA, USA) with monochromated Al K $\alpha$  X-ray source, and the binding energies were recorded with a 0.05 eV step. The binding energies were aligned with respect to the C1s peak (285.0 eV), and the O1s and C1s peaks were deconvoluted and fitted using CasaXPS software (version 2.3.19) with Shirley background.

#### 2.4. Electrochemical Measurements

All electrochemical measurements were taken using a BioLogic SP-300 potentiostat and EC-Lab software. Cyclic voltammetry (CV) was conducted in 0.5 M HBr solution between 0 and 1.5 V vs. Ag/AgCl. The electrochemical performance of the electrodes was investigated using linear sweep voltammetry (LSV), polarisation and galvanostatic oxidation/reduction cycling in 3 M HBr/1 M Br<sub>2</sub> electrolytes. LSV measurements were performed in the range of 0.2 to 0.95 V vs. Ag/AgCl at a scan rate of 1 mV s<sup>-1</sup> to obtain the kinetic parameters for different carbon materials. Polarisation studies were completed with cut-off potentials ( $V_{\text{cutoff}}$ ) of 1.2 V and 0.4 V vs. Ag/AgCl for oxidation and reduction, respectively. Finally, to test the stability of the carbon materials, cycling tests were conducted over 50 cycles at 100 mA cm<sup>-2</sup> for 10 min during oxidation, and at -100 mA cm<sup>-2</sup> for 10 min during reduction, with  $V_{\text{cutoff}}$  of 1.2 V for oxidation and 0.4 V for reduction. During the tests, the electrolyte was stirred throughout at 400 rpm using a Camlab MS-H280-Pro magnetic stirrer (Cambridge, UK) and a PTFE stir bar in order to minimise diffusion limitations. For capacitance measurements, CV was conducted at  $\pm 50$  mV vs. open circuit voltage (OCV) in 1 M KCl electrolyte, from 0.9 V to 1.0 V vs. Ag/AgCl. Eight potential scan rates were used between 20 mV s<sup>-1</sup> and 200 mV s<sup>-1</sup>. Anodic,  $iC_a$ , and cathodic,  $iC_c$ , charging currents were taken at 0.95 V vs. Ag/AgCl. All experimentation was conducted at 25 °C.

### 3. Results and Discussion

#### 3.1. SEM Characterisation

The effect of thermal oxidation on the surface morphology of the carbon materials was examined by SEM, as shown in Figure 2. The SGL 22AA carbon paper displays a perceptible increase in surface roughness after thermal oxidation (Figure 2b) when compared to the pristine sample (Figure 2a) caused by the introduction of small defects on the surface of the carbon fibres. This leads to an increase in surface area and the number of active sites for the Br<sub>2</sub>/Br<sup>-</sup> reaction, facilitating improved electrochemical performance following thermal oxidation [17,29,30]. As shown in Figure 3, a similar modification of surface morphology is observed in the SGL 28AA carbon paper, while little or no change is seen in the case of the SGL 36AA carbon paper.

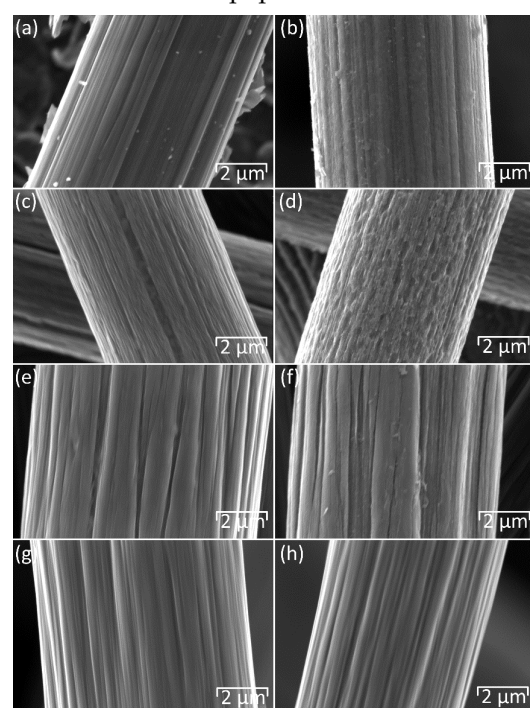


**Figure 2.** SEM images of materials before (a,c,e,g) and after (b,d,f,h) thermal oxidation at 550 °C for 5 h: (a,b) 22AA, (c,d) MGL370, (e,f) carbon cloth, (g,h) GF. Magnification 20,000Accelerating voltage 5 kV. Working distance 14 mm.

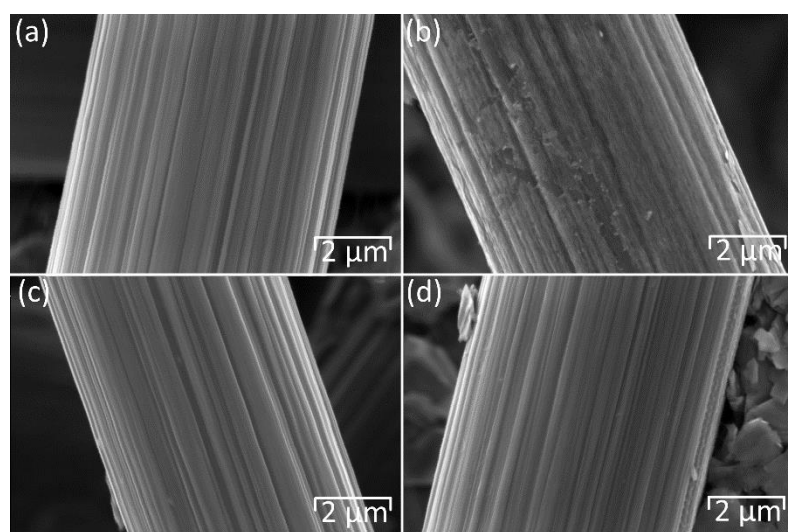


**Figure 3.** SEM images of materials before (a,c) and after (b,d) thermal oxidation at 550 °C for 5 h: (a,b) 28AA, (c,d) 36AA. Magnification 20 k. Accelerating voltage 5 kV. Working distance 14 mm.

The change in surface morphology is particularly pronounced for the MGL370 moulded graphite laminate, which exhibits surface defects in the as-received condition (Figure 2c). Thermal oxidation results in the coalescence of small surface defects to produce larger surface cavities on the graphite fibres (Figure 2d), as previously observed by Wu et al. [17]. The difference between pristine and thermally treated samples is less distinct in the case of the carbon cloth (Figure 2e,f) and graphite felt (Figure 2g,h), although some increase in the number of defects and surface roughness is observable. In the case of graphite felt, fibre diameter appears reduced from around 8  $\mu\text{m}$  for the pristine sample (Figure 2g) to around 6  $\mu\text{m}$  after heat treatment (Figure 2h). As discussed in Section 3.3, the increase in surface roughness, development of surface cavities, subsequent reduction in fibre diameter and associated mass loss (Table S1) following thermal treatment are due to the oxidation of O–C=O to CO<sub>2</sub>, which escapes as gas from the sample [19,31].

### 3.2. Electrochemical Characterisation

Cyclic voltammograms obtained on the 22AA carbon paper at varying potential scan rates are provided in Figure 4. The bromine electrode proceeds according to Equation (1) [32]. Anodic current density peaks are observed for the oxidation of bromide to bromine, with the peak potentials becoming more positive with increasing scan rates.



During reduction, the cathodic current peaks are seen to become more negative with increasing scan rates. In addition, two reduction peaks are observed for all the scan rates employed, these being particularly clear at low scan rates of 10 and 20  $\text{mV s}^{-1}$ , due to the formation of tribromide ions [33–35], leading to reaction (2) [32]. The dependency of both anodic and cathodic peak potentials on scan rate,  $\nu$ , and the proportionality of peak current densities to  $\nu^{1/2}$  (inset, Figure 4) confirm the quasi-reversible nature of the bromine electrode reaction [36,37].



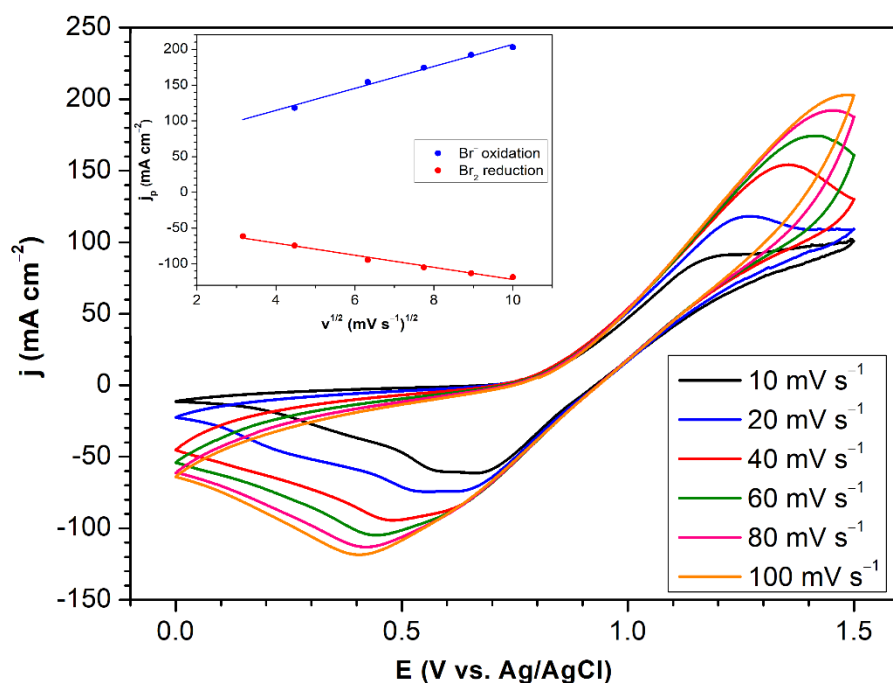


**Figure 4.** Cyclic voltammograms obtained at varying potential scan rates on an SGL 22AA carbon paper working electrode. Inset: plots of peak current density vs. square root of scan rate. 1 M HBr electrolyte, working electrode area  $0.1\text{ cm}^2$ . Temperature  $25^\circ\text{C}$ .

The kinetic parameters for the Br $_2$ /Br $^-$  reactions on the carbon materials under investigation were obtained by LSV (Figure 5). The steady state polarisation theory predicts that the relationship between overpotential and current density is linear at low overpotentials ( $\eta < 25\text{ mV}$ ) [38–40]. Charge transfer resistances,  $R_{ct}$ , exchange current densities,  $i_0$ , and reaction rate constants,  $k_0$ , were calculated for each of the materials before and after thermal treatment according to Equations (3)–(5). Here,  $\eta$  is the overpotential, calculated by subtraction of the observed equilibrium potential from the working electrode potential [41];  $j$  is the current density;  $R$  is the universal gas constant;  $T$  is the temperature in Kelvin;  $n$  is the number of electrons transferred per mole of reactant;  $F$  is the Faraday constant; and  $C_0$  is the reactant concentration [39,40]. The results are listed in Table 2. Here, the apparent charge transfer resistance, exchange current density and reaction rate constant values are defined by the combined effects of electrode geometry and catalytic capability.

$$R_{ct} = \eta / j \quad (3)$$

$$i_0 = RT / nFR_{ct} \quad (4)$$

$$k_0 = i_0 / nFC_0 \quad (5)$$

In all cases, the thermally oxidised carbon materials show superior kinetic parameters when compared to the as-received samples. The formation of oxygen-containing functional groups on the surface of carbon materials during thermal treatment in air has been reported previously [17,19,29–31]. This improves the activity for the Br $_2$ /Br $^-$  reactions in two ways. Firstly, the presence of hydroxyl and carboxyl groups in particular increase the polarity and hydrophilicity of the material [19,30,31,42]. Secondly, the evolution of carbon monoxide/dioxide increases the surface roughness of the material, and therefore, the availability of the active reaction sites [17,19,29,30], as shown by the results of SEM provided in Figure 2.

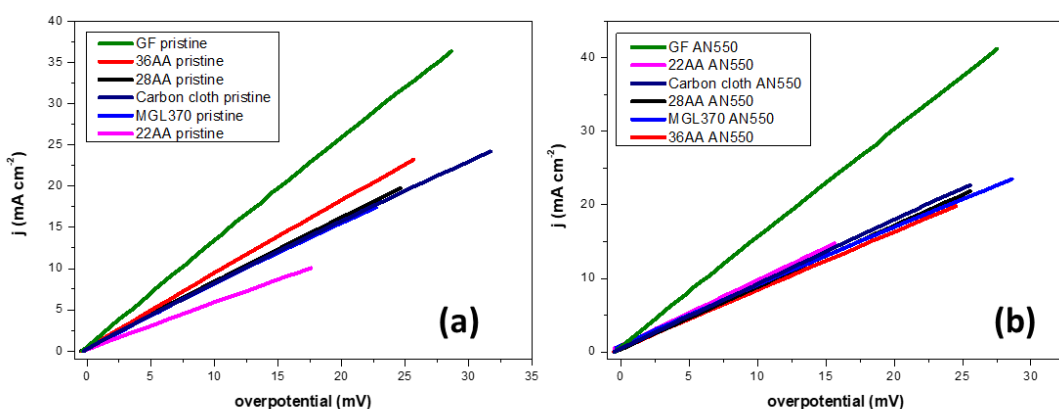


**Figure 5.** (a) LSV curves for pristine samples, (b) LSV curves for annealed samples at scan rate of 1 mV/s. 3 M HBr/1 M Br<sub>2</sub> electrolyte, working electrode area 0.1 cm<sup>2</sup>. Temperature 298 K.

**Table 2.** Kinetic parameters of the bromine reduction reaction and capacitances for different carbon materials (pristine and annealed).

Electrode Material	R <sub>ct</sub> ( $\Omega$ cm <sup>2</sup> )	i <sub>0</sub> (mA cm <sup>-2</sup> )	k <sub>0</sub> $\times$ 10 <sup>-5</sup> (cm s <sup>-1</sup> )	C <sub>dl</sub> ( $\mu$ F)
22AA pristine	1.78	7.26	3.76	59.5
28AA pristine	1.32	9.79	5.07	85.0
36AA pristine	1.28	10.09	5.23	86.5
MGL370 pristine	1.33	9.71	5.03	68.0
GF pristine	0.80	16.19	8.39	117.8
Carbon cloth pristine	1.32	9.79	5.07	99.1
22AA AN550	1.12	11.52	5.97	662.2
28AA AN550	1.19	10.86	5.63	756.6
36AA AN550	1.26	10.24	5.31	845.1
MGL370 AN550	1.25	10.33	5.35	608.2
GF AN550	0.68	18.97	9.83	2440.0
Carbon cloth AN550	1.14	11.31	5.86	1395.0

Graphite felt exhibits the lowest charge transfer resistance, highest exchange current density and highest reaction rate constant of all the materials tested in both pristine and thermally oxidised conditions. Following thermal oxidation, the graphite felt sample, GF AN550, displays a low charge transfer resistance (R<sub>ct</sub>) of 0.68  $\Omega$  cm<sup>2</sup> and high exchange current density (i<sub>0</sub>) and reaction rate constant (k<sub>0</sub>) of 18.97 mA cm<sup>-2</sup> and 9.83  $\times$  10<sup>-5</sup> cm s<sup>-1</sup>, respectively. The R<sub>ct</sub> value of GF AN550 is the lowest reported in the literature among bromine electrode materials, such as acetylene black, carbon nanotube, expanded graphite and BP2000 [12], while the i<sub>0</sub> and k<sub>0</sub> values are comparable to the state-of-the-art bromine carbon electrodes [4,11–13]. The other materials investigated demonstrate similar performance after thermal oxidation, with charge transfer resistances ranging from 1.12 to 1.26  $\Omega$  cm<sup>2</sup>, exchange current densities between 10.24 and 11.52 mA cm<sup>-2</sup> and reaction rate constants from 5.31  $\times$  10<sup>-5</sup> to 5.97  $\times$  10<sup>-5</sup> cm s<sup>-1</sup>. While the MGL370 and carbon cloth may be expected to provide improved performance when compared to the SGL carbon papers due to their larger thicknesses, the porosity of these materials is reduced in comparison, at 78% and 80%, respectively (Table 1). This may reduce the electrolyte penetration into these materials, reducing the surface area available for the Br<sub>2</sub>/Br<sup>−</sup> reactions, thus restricting the current densities observed in Figure 5. The LSV results clearly indicate that thermal oxidation is beneficial to the electrocatalytic performance of the materials investigated for the Br<sub>2</sub>/Br<sup>−</sup> reactions. Hence, only these samples are studied further.

The plots displayed in Figure 5 do not represent the intrinsic activity of the carbon materials and are influenced by the contributions from their respective surface areas. The electrochemical surface areas (ECSA) of the carbon materials were estimated by determining the value of double layer capacitance (C<sub>dl</sub>). High C<sub>dl</sub> values are indicative of superior ECSA, thereby implying a higher number of available active sites for the bromine reaction. Figures S1 and S2 demonstrate the CV curves for the carbon materials (pristine and thermally treated at 550 °C) at various scan rates. From these graphs, the cathodic and anodic current

densities were plotted against the respective scan rates to determine the value of  $C_{dl}$ . As seen in Table 2 (derived from Figure 6, Figures S1 and S2), the value of  $C_{dl}$  ( $2440 \mu F$ ) is the highest for GF AN550. The increase in  $C_{dl}$  for GF is  $21\times$  upon thermal treatment, whereas the other carbon materials have an increase in the range of  $9\text{--}14\times$ . Hence, the capacitance measurements show that upon thermal treatment, the GF provides the maximum number of active sites for the  $\text{Br}_2/\text{Br}^-$  reactions among the carbon materials tested. The enhanced ECSA can thus be confirmed as one of the reasons for the superior performance of GF AN550, as seen in LSV measurements. Figure 7 provides the polarisation curves for the thermally treated electrode materials in order to ascertain the achievable oxidation and reduction current densities. Cut-off potentials,  $V_{cutoff}$ , of 1.2 V vs. Ag/AgCl for oxidation and 0.4 V vs. Ag/AgCl for reduction were applied to mimic the conditions in an  $\text{H}_2\text{-Br}_2$  flow cell. At low current densities, the charge and discharge polarisation curves are linear. As expected, following the results of LSV, the best performance is achieved with thermally oxidised graphite felt, GF AN550, which displays the capacity for oxidation and reduction with current densities of  $640 \text{ mA cm}^{-2}$  and  $430 \text{ mA cm}^{-2}$ , respectively, within the applied potential limits. The other electrode materials exhibit oxidation and reduction current densities in the range of  $350\text{--}400 \text{ mA cm}^{-2}$  and  $290\text{--}300 \text{ mA cm}^{-2}$ , respectively, within the same potential limits. The significant performance of GF AN550 in achieving such high current densities makes it a promising bromine electrode candidate.

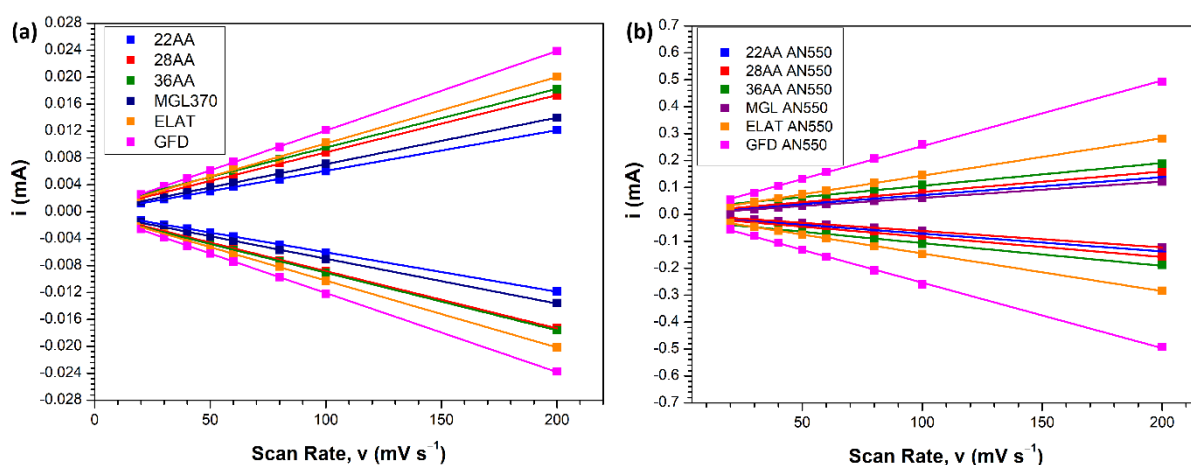


**Figure 6.** Plots of  $iC_a$  and  $iC_c$  vs.  $v$  on (a) as-received electrode materials (b) materials thermally oxidised at  $550\text{ }^\circ\text{C}$  for 5 h. 1 M KCl electrolyte. Working electrode area  $0.1 \text{ cm}^2$ . Temperature  $25\text{ }^\circ\text{C}$ .

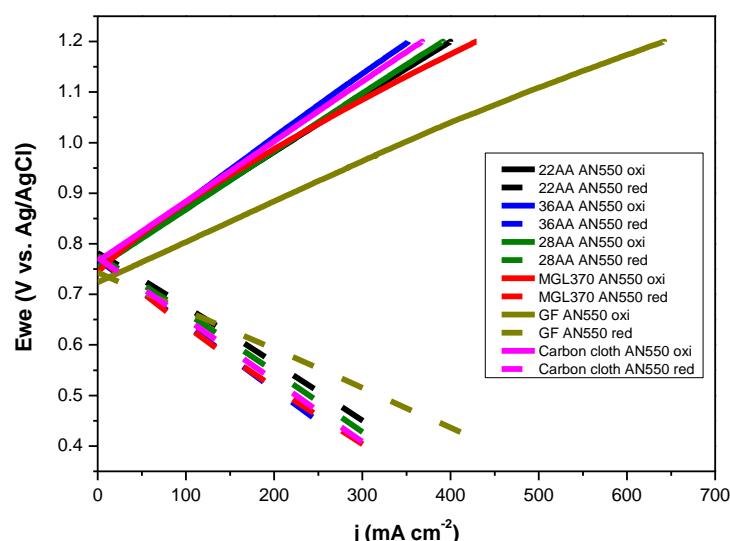


**Figure 7.** Polarisation curves for the annealed carbon materials. 3 M HBr/1 M  $\text{Br}_2$  electrolyte, working electrode area  $0.1 \text{ cm}^2$ . Temperature  $25\text{ }^\circ\text{C}$ .

Bromine electrode oxidation/reduction cycling was conducted in a stirred electrolyte solution of 3 M HBr/1 M Br<sub>2</sub> to evaluate the performance and stability of the thermally oxidised carbon materials. Each cycle comprised oxidation for 10 min at 100 mA cm<sup>-2</sup> followed by reduction for 10 min at -100 mA cm<sup>-2</sup> with potential limits, V<sub>cutoff</sub>, of 1.2 V and 0.4 V vs. Ag/AgCl for oxidation and reduction, respectively. The potential responses are reported in Figure 8, and their corresponding reduction/oxidation potential ratios are listed in Table 3. As shown in Figure 8b,d, all the materials provide stable performance over the period of 50 cycles. The highest reduction/oxidation potential ratios are achieved on the GF AN550 electrode, indicating the lowest reaction overpotentials and possibility of improved voltaic efficiencies in the H<sub>2</sub>-Br<sub>2</sub> flow cell. This is commensurate with the improved kinetic parameters obtained from the LSV results and the higher current densities observed in Figure 7, reflecting the combined effect of high ECSA and hydrophilicity achieved by thermal oxidation and the intrinsic catalytic activity of GF. As shown in Table 3, the MGL370 AN550 electrode displays the lowest reduction/oxidation potential ratios, which, again, corresponds to the lowest current densities in Figure 7, plus the lowest exchange current density and reaction rate constant and highest charge transfer resistance from the LSV results.

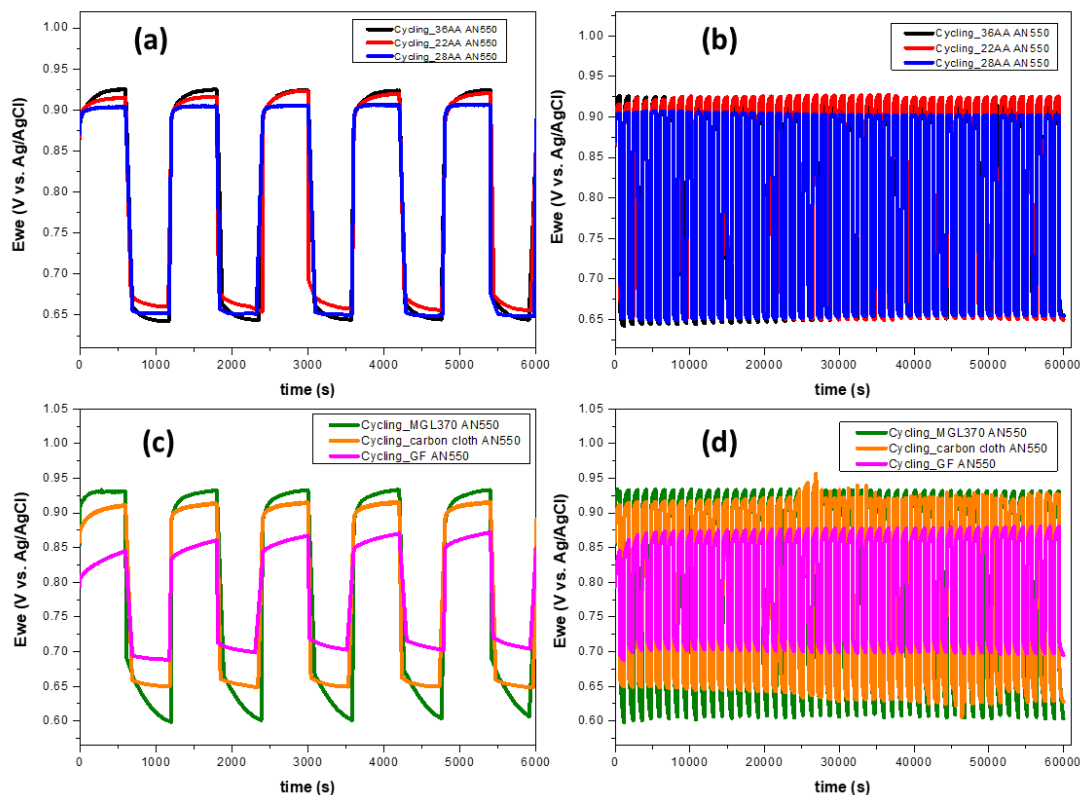


**Figure 8.** Potential responses during bromine oxidation/reduction at  $\pm 100 \text{ mA cm}^{-2}$  for 10 min on annealed carbon electrode materials; (a,c) the first 5 cycles, (b,d) 50 cycles. 3 M HBr/1 M Br<sub>2</sub> electrolyte, working electrode area  $0.1 \text{ cm}^2$ . Temperature 25 °C.

**Table 3.** Reduction to oxidation potential ratios of bromine electrode reaction obtained from the annealed carbon samples.

Electrode Material	Reduction/Oxidation Potential Ratio (1st Cycle)	Reduction/Oxidation Potential Ratio (50th Cycle)
22AA AN550	0.73	0.72
28AA AN550	0.72	0.73
36AA AN550	0.70	0.73
MGL370 AN550	0.67	0.69
GF AN550	0.83	0.80
Carbon cloth AN550	0.72	0.70

Thermally oxidised graphite felt clearly exhibits the best performance as a bromine electrode among the carbon materials tested in this work. However, previous literature reports the use of carbon papers as bromine electrodes in H<sub>2</sub>-Br<sub>2</sub> systems [10,18,43,44]. Tucker et al. have previously made a direct comparison of carbon paper, foam and cloth in an H<sub>2</sub>-Br<sub>2</sub> flow cell, reporting increased area-specific resistances (ASR) in the case of foam and cloth, with the latter causing high resistance to electrolyte flow due to its lower porosity [43]. While no previous report of direct comparison between the felts and papers in H<sub>2</sub>-Br<sub>2</sub> flow cells is known, graphite felts have been utilised successfully as bromine electrodes in the Zn-Br system [16,28]. Nevertheless, it is prudent to highlight the need for further study and modified cell design to enable optimal utilisation of graphite felts as bromine electrodes in H<sub>2</sub>-Br<sub>2</sub> flow cells.

### 3.3. XPS Analysis

XPS was conducted on the best performing graphite felt electrodes, both in the as-received condition and after thermal oxidation at 550 °C for 5 h. Figure 9 provides the wide survey spectra showing the C1s and O1s peaks. The relative intensity and FWHM of these peaks were used to calculate the atomic percentage of oxygen present in the samples, with the results presented in Table 4. Figure 10a,b display the high-resolution C1s peaks, deconvoluted to components at 284.5 eV corresponding to graphitic carbon (C=C), 285.5 eV assigned to aliphatic hydrocarbons (C-C), phenolic (C-O) at 286.5 eV, carbonyl and carboxyl (C=O) at 287.5 eV and O-C=O at 289.5 eV [29,42,45,46]. In addition, for the thermally oxidised graphite felt (Figure 10b), a small peak is observed at 291 eV, attributed to the π–π interaction of graphite [29]. The high-resolution O1s peaks at 533 eV in Figure 10c,d are deconvoluted into three components: carbonyl and carboxyl (C=O) at 531.5 eV, phenolic (C-O) at 532.5 eV and O-C=O at around 534 eV [29,30,42], and the resultant distribution of these species is given in Table 4.

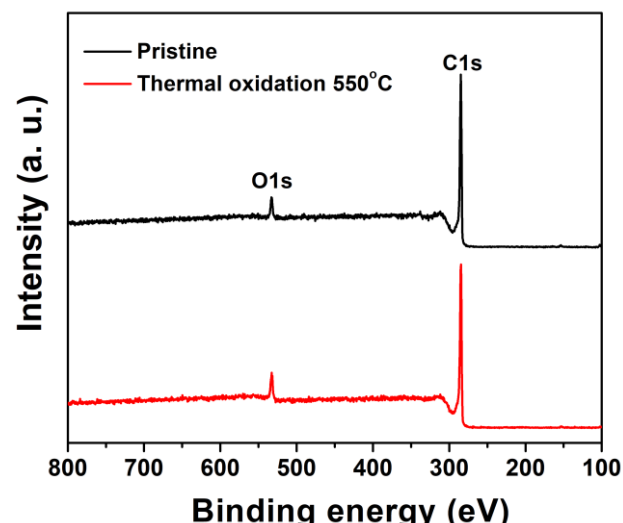


**Figure 9.** XPS survey spectra of graphite felt in as-received condition and after thermal oxidation at 550 °C for 5 h.

**Table 4.** Oxygen functional group content and distribution on GF samples.

Sample	Oxygen Functional Group Content (%)	Oxygen Functional Group Distribution from O1s Spectra (%)		
		C=O	C–O	O–C=O
GF	16.56	4.73	33.59	61.69
GF AN550	16.86	10.90	62.34	26.76

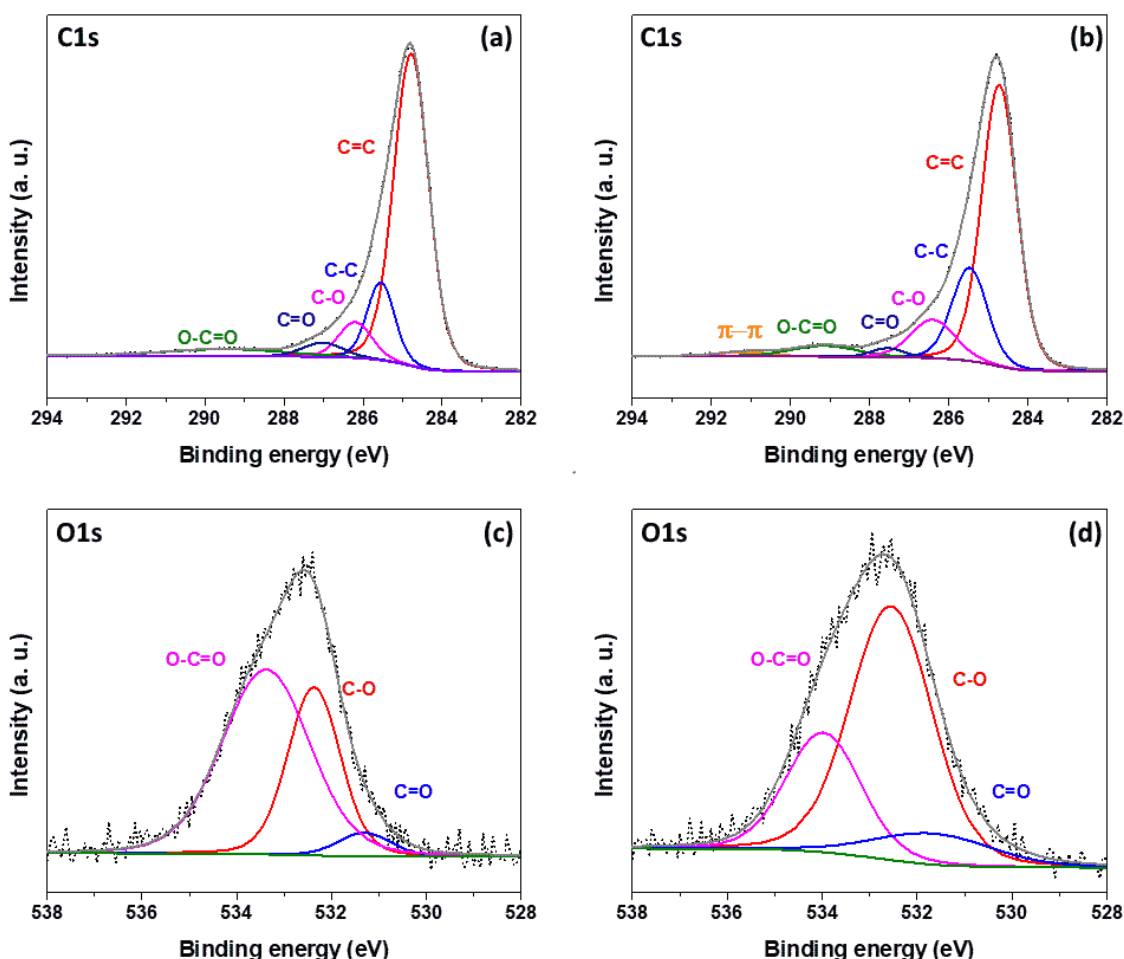


**Figure 10.** Deconvoluted spectra of graphite felt before (a,c) and after (b,d) thermal oxidation at 550 °C for 5 h: (a,b) C1s spectra, (c,d) O1s spectra.

The GF AN550 sample displays an oxygen functional group content of 16.86%, only a marginal increase compared to the 16.56% observed for the as-received GF sample (Table 4, Figure 9). However, the distribution of oxygen-containing functional groups is significantly shifted by the thermal oxidation treatment, as shown by the deconvoluted O1s spectra in Figure 10c,d. The O-C=O content reduces dramatically from 61.69% prior to thermal oxidation to 26.76% for the GF AN550 sample (Table 4), this being due to the further oxidation of O-C=O to carbon dioxide [46], leading to loss of mass from the graphite felt and the reduced fibre diameter observed in the SEM images in Figure 2g,h. Conversely, the proportion of both C-O and C=O increases after thermal treatment, from 33.59% to 62.34% in the case of phenolic (C-O) groups, and from 4.73% to 10.90% for carboxyl and carbonyl (C=O) groups. C-O groups are formed by the breakage of C=C bonds, indicated by the reduction in the graphitic C=C peak in the C1s spectra following oxidation (Figure 10a,b), and C=O groups result from further oxidation of C-O [19].

The improved performance of graphite felt following thermal oxidation is therefore attributed not only to the increased ECSA but also to the increased presence of carboxyl, carbonyl and phenolic functional groups on the fibre surface. These increase the polarity of the graphite felt surface, improving the hydrophilicity and adsorption ability of the material [19,30,31], thus providing active sites for the bromine electrode reaction. The limitation of the current study includes electrode–electrolyte interfacial studies and the effect of material treatment during manufacturing. These studies will deepen our understanding about the key electrode characteristics that dictate the performance of a given material in a flow cell.

#### 4. Conclusions

Thermally oxidised carbon electrodes exhibit superior electrocatalytic performance for  $\text{Br}_2/\text{Br}^-$  redox reactions compared to the as-received materials, a feature attributed to the formation of carboxyl, carbonyl and phenolic oxygen-containing functional groups under heating in air, causing an increase in surface area and hydrophilicity of the electrodes. The study of kinetic parameters by linear sweep voltammetry along with polarisation studies provide conclusive evidence in determining the enhancement of catalytic activity over pristine carbon materials. A graphite felt electrode oxidised at 550 °C for 5 h significantly outperformed the other carbon paper and cloth materials investigated. A low charge transfer resistance of  $0.68 \Omega \text{ cm}^2$  was observed for this material, along with high exchange current density and reaction rate constant of  $18.97 \text{ mA cm}^{-2}$  and  $9.83 \times 10^{-5} \text{ cm s}^{-1}$ , respectively. Bromine electrode half-cell cycling tests demonstrate the stability of the thermally treated carbon materials over 50 oxidation/reduction cycles with the highest reduction/oxidation potential ratios in excess of 0.8 observed for the thermally oxidised graphite felt electrode. Further work will include investigating the effect of preparatory treatments on the performance of the graphite felt as a bromine electrode; verifying the performance in an  $\text{H}_2\text{-Br}_2$  flow cell with flow through bromine electrode configuration; and evaluating the effect of electrolyte temperature on the reaction kinetics of graphite felt. This work is currently in progress and will be reported in subsequent publications.

**Supplementary Materials:** The following supporting information can be downloaded at: <https://www.mdpi.com/article/10.3390/batteries8100166/s1>, Figure S1: Cyclic voltammograms obtained on as received electrode materials at varying potential sweep rates between 0.9 V and 1.0 V vs.  $\text{Ag}/\text{AgCl}$  in 1M KCl solution (a) 22AA (b) 28AA (c) 36AA (d) MGL370 (e) ELAT (f) GFD. Working electrode area  $0.1 \text{ cm}^2$ . Temperature 25 °C; Figure S2: Cyclic voltammograms obtained on electrode materials after thermal oxidation at 550 °C for 5 hours at varying potential sweep rates between 0.9 V and 1.0 V vs.  $\text{Ag}/\text{AgCl}$  in 1M KCl solution (a) 22AA (b) 28AA (c) 36AA (d) MGL370 (e) ELAT (f) GFD. Working electrode area  $0.1 \text{ cm}^2$ . Temperature 25 °C; Table S1: Mass of electrode materials before and after thermal oxidation at 550 °C and percentage mass loss.

**Author Contributions:** Conceptualization, Y.P.; D.P.T.; and X.L.; methodology, Y.P.; D.P.T. and X.L.; formal analysis, Y.P. and D.P.T.; investigation, Y.P.; and D.P.T.; resources, X.L.; data curation, Y.P., D.P.T. and A.A.; writing—original draft preparation, Y.P.; writing—review and editing, Y.P., D.P.T., X.L. and A.A.; supervision, X.L. and M.E.S.; project administration, X.L. and P.C.; funding acquisition, X.L. and M.E.S. All authors have read and agreed to the published version of the manuscript.

**Funding:** This work has received funding support from the European Union’s Horizon 2020 research and innovation programme under grant agreement No 875524, the EPSRC Supergen Energy Storage Project (grant number: EP/P003494/1) and the Royal Academy of Engineering UK-Germany Energy Systems Symposium Award (UKDE\100005). We would like to thank all our project partners for the valuable discussions and insights.

**Conflicts of Interest:** The authors declare no conflict of interest.

#### References

1. IEA. *World Energy Balances: Overview*; IEA: Paris, France, 2019.
2. IEA. *Global Energy Review*; IEA: Paris, France, 2021.
3. Leung, P.; Li, X.; de León, C.P.; Berlouis, L.; Low, C.T.J.; Walsh, F.C. Progress in redox flow batteries, remaining challenges and their applications in energy storage. *RSC Adv.* **2012**, *2*, 10125–10156. [[CrossRef](#)]
4. Wang, C.; Lai, Q.; Feng, K.; Xu, P.; Li, X.; Zhang, H. From zeolite-type metal organic framework to porous nano-sheet carbon: High activity positive electrode material for bromine-based flow batteries. *Nano Energy* **2018**, *44*, 240–247. [[CrossRef](#)]
5. Dunn, B.; Kamath, H.; Tarascon, J.-M. Electrical Energy Storage for the Grid: A Battery of Choices. *Science* **2011**, *334*, 928–935. [[CrossRef](#)] [[PubMed](#)]
6. United States Geological Survey. *Mineral Commodity Summaries 2019*; U.S Geological Survey: Reston, VA, USA, 2019; pp. 1–199. [[CrossRef](#)]
7. Kosek, J.; Laconti, A. Advanced hydrogen electrode for a hydrogen-bromine battery. *J. Power Sources* **1988**, *22*, 293–300. [[CrossRef](#)]
8. Saadi, K.; Nanikashvili, P.; Tatus-Portnoy, Z.; Hardisty, S.; Shokhen, V.; Zysler, M.; Zitoun, D. Crossover-tolerant coated platinum catalysts in hydrogen/bromine redox flow battery. *J. Power Sources* **2019**, *422*, 84–91. [[CrossRef](#)]

9. Barna, G.G.; Frank, S.N.; Teherani, T.H.; Weedon, L.D. Lifetime Studies in H<sub>2</sub>/Br<sub>2</sub> Fuel Cells. *J. Electrochem. Soc.* **1984**, *131*, 1973–1980. [[CrossRef](#)]
10. Cho, K.T.; Ridgway, P.; Weber, A.; Haussener, S.; Battaglia, V.; Srinivasan, V. High Performance Hydrogen/Bromine Redox Flow Battery for Grid-Scale Energy Storage. *J. Electrochem. Soc.* **2012**, *159*, A1806–A1815. [[CrossRef](#)]
11. Wang, C.; Li, X.; Xi, X.; Zhou, W.; Lai, Q.; Zhang, H. Bimodal highly ordered mesostructure carbon with high activity for Br<sub>2</sub>/Br<sup>−</sup> redox couple in bromine based batteries. *Nano Energy* **2016**, *21*, 217–227. [[CrossRef](#)]
12. Wang, C.; Li, X.; Xi, X.; Xu, P.; Lai, Q.; Zhang, H. Relationship between activity and structure of carbon materials for Br<sub>2</sub>/Br<sup>−</sup> in zinc bromine flow batteries. *RSC Adv.* **2016**, *6*, 40169–40174. [[CrossRef](#)]
13. Wang, C.; Lai, Q.; Xu, P.; Zheng, D.; Li, X.; Zhang, H. Cage-Like Porous Carbon with Superhigh Activity and Br<sub>2</sub>-Complex-Entrapping Capability for Bromine-Based Flow Batteries. *Adv. Mater.* **2017**, *29*, 1605815. [[CrossRef](#)]
14. Wang, S.; Liang, Y.; Zhuo, W.; Lei, H.; Javed, M.S.; Liu, B.; Wang, Z.; Mai, W. Freestanding polypyrrole/carbon nanotube electrodes with high mass loading for robust flexible supercapacitors. *Mater. Chem. Front.* **2020**, *5*, 1324–1329. [[CrossRef](#)]
15. Wu, M.; Zhao, T.; Zhang, R.; Jiang, H.; Wei, L. A Zinc-Bromine Flow Battery with Improved Design of Cell Structure and Electrodes. *Energy Technol.* **2017**, *6*, 333–339. [[CrossRef](#)]
16. Suresh, S.; Ulaganathan, M.; Venkatesan, N.; Periasamy, P.; Ragupathy, P. High performance zinc-bromine redox flow batteries: Role of various carbon felts and cell configurations. *J. Energy Storage* **2018**, *20*, 134–139. [[CrossRef](#)]
17. Wu, M.C.; Zhao, T.S.; Jiang, H.R.; Zeng, Y.K.; Ren, Y.X. High-performance zinc bromine flow battery via improved design of electrolyte and electrode. *J. Power Sources* **2017**, *355*, 62–68. [[CrossRef](#)]
18. Cho, K.T.; Tucker, M.C.; Ding, M.; Ridgway, P.; Battaglia, V.S.; Srinivasan, V.; Weber, A.Z. Cyclic Performance Analysis of Hydrogen/Bromine Flow Batteries for Grid-Scale Energy Storage. *ChemPlusChem* **2014**, *80*, 402–411. [[CrossRef](#)]
19. Zhang, L.; Shao, Z.-G.; Wang, X.; Yu, H.; Liu, S.; Yi, B. The characterization of graphite felt electrode with surface modification for H<sub>2</sub>/Br<sub>2</sub> fuel cell. *J. Power Sources* **2013**, *242*, 15–22. [[CrossRef](#)]
20. Zhou, H.; Zhang, H.; Zhao, P.; Yi, B. A comparative study of carbon felt and activated carbon based electrodes for sodium polysulfide/bromine redox flow battery. *Electrochim. Acta* **2006**, *51*, 6304–6312. [[CrossRef](#)]
21. Javed, M.S.; Shah, S.S.A.; Najam, T.; Siyal, S.H.; Hussain, S.; Saleem, M.; Zhao, Z.; Mai, W. Achieving high-energy density and superior cyclic stability in flexible and lightweight pseudocapacitor through synergic effects of binder-free CoGa<sub>2</sub>O<sub>4</sub> 2D-hexagonal nanoplates. *Nano Energy* **2020**, *77*, 105276. [[CrossRef](#)]
22. Javed, M.S.; Shaheen, N.; Hussain, S.; Li, J.; Shah, S.S.A.; Abbas, Y.; Ahmad, M.A.; Raza, R.; Mai, W. An ultra-high energy density flexible asymmetric supercapacitor based on hierarchical fabric decorated with 2D bimetallic oxide nanosheets and MOF-derived porous carbon polyhedra. *J. Mater. Chem. A* **2018**, *7*, 946–957. [[CrossRef](#)]
23. Le, T.X.H.; Bechelany, M.; Cretin, M. Carbon felt based-electrodes for energy and environmental applications: A review. *Carbon* **2017**, *122*, 564–591. [[CrossRef](#)]
24. Wang, M.; Du, J.; Zhou, J.; Ma, C.; Bao, L.; Li, X.; Li, X. Numerical evaluation of the effect of mesopore microstructure for carbon electrode in flow battery. *J. Power Sources* **2019**, *424*, 27–34. [[CrossRef](#)]
25. Zhou, X.; Zhao, T.; Zeng, Y.; An, L.; Wei, L. A highly permeable and enhanced surface area carbon-cloth electrode for vanadium redox flow batteries. *J. Power Sources* **2016**, *329*, 247–254. [[CrossRef](#)]
26. dos Reis, G.; de Oliveira, H.; Larsson, S.; Thyrel, M.; Lima, E.C. A Short Review on the Electrochemical Performance of Hierarchical and Nitrogen-Doped Activated Biocarbon-Based Electrodes for Supercapacitors. *Nanomaterials* **2021**, *11*, 424. [[CrossRef](#)]
27. Du, Y.; Ma, S.; Dai, J.; Lin, J.; Zhou, X.; Chen, T.; Gu, X. Biomass Carbon Materials Contribute Better Alkali-Metal–Selenium Batteries: A Mini-Review. *Batteries* **2022**, *8*, 123. [[CrossRef](#)]
28. Lai, Q.; Zhang, H.; Li, X.; Zhang, L.; Cheng, Y. A novel single flow zinc–bromine battery with improved energy density. *J. Power Sources* **2013**, *235*, 1–4. [[CrossRef](#)]
29. Dixon, D.; Babu, D.; Langner, J.; Bruns, M.; Pfaffmann, L.; Bhaskar, A.; Schneider, J.; Scheiba, F.; Ehrenberg, H. Effect of oxygen plasma treatment on the electrochemical performance of the rayon and polyacrylonitrile based carbon felt for the vanadium redox flow battery application. *J. Power Sources* **2016**, *332*, 240–248. [[CrossRef](#)]
30. Kim, K.J.; Kim, Y.-J.; Kim, J.-H.; Park, M.-S. The effects of surface modification on carbon felt electrodes for use in vanadium redox flow batteries. *Mater. Chem. Phys.* **2011**, *131*, 547–553. [[CrossRef](#)]
31. Sun, B.; Skyllas-Kazacos, M. Modification of graphite electrode materials for vanadium redox flow battery application—I. Thermal treatment. *Electrochimica Acta* **1992**, *37*, 1253–1260. [[CrossRef](#)]
32. Parsons, R.; Bard, A.J.; Parsons, R.; Jordan, J. *Standard Potentials in Aqueous Solution*, 1st ed.; M. Dekker: New York, NY, USA, 1985; pp. 13–37.
33. Mastragostino, M.; Gramellini, C. Kinetic study of the electrochemical processes of the bromine/bromine aqueous system on vitreous carbon electrodes. *Electrochim. Acta* **1985**, *30*, 373–380. [[CrossRef](#)]
34. Ramette, R.W.; Palmer, D.A. Thermodynamics of tri- and pentabromide anions in aqueous solution. *J. Solut. Chem.* **1986**, *15*, 387–395. [[CrossRef](#)]
35. Küttinger, M.; Włodarczyk, J.K.; Daubner, D.; Fischer, P.; Tübke, J. High energy density electrolytes for H<sub>2</sub>/Br<sub>2</sub> redox flow batteries, their polybromide composition and influence on battery cycling limits. *RSC Adv.* **2021**, *11*, 5218–5229. [[CrossRef](#)] [[PubMed](#)]

36. Vogel, I.; Möbius, A. On some problems of the zinc—Bromine system as an electric energy storage system of higher efficiency—I. Kinetics of the bromine electrode. *Electrochim. Acta* **1991**, *36*, 1403–1408. [[CrossRef](#)]
37. Pletcher, D. *An Introduction to Electrode Reactions*, in: *A First Course Electrode Process*, 2nd ed.; RSC Publishing: Cambridge, UK, 2009; p. 45.
38. Rahman, F.; Skyllas-Kazacos, M. Vanadium redox battery: Positive half-cell electrolyte studies. *J. Power Sources* **2009**, *189*, 1212–1219. [[CrossRef](#)]
39. Wu, X.; Liu, S.; Wang, N.; Peng, S.; He, Z. Influence of organic additives on electrochemical properties of the positive electrolyte for all-vanadium redox flow battery. *Electrochim. Acta* **2012**, *78*, 475–482. [[CrossRef](#)]
40. Bard, A.; Faulkner, L. Kinetics of Electrode Reactions. In *Electrochem. Methods Fundam. Appl.*, 2nd ed.; John Wiley & Sons Inc.: New York, NY, USA, 2001; pp. 87–136.
41. Bard, A.; Faulkner, L. Introduction and Overview of Electrode Processes. In *Electrochem. Methods Fundam. Appl.*, 2nd ed.; John Wiley & Sons Inc.: New York, NY, USA, 2001; pp. 1–43.
42. Yue, L.; Li, W.; Sun, F.; Zhao, L.; Xing, L. Highly hydroxylated carbon fibres as electrode materials of all-vanadium redox flow battery. *Carbon* **2010**, *48*, 3079–3090. [[CrossRef](#)]
43. Tucker, M.C.; Cho, K.T.; Weber, A.Z.; Lin, G.; Van Nguyen, T. Optimization of electrode characteristics for the Br<sub>2</sub>/H<sub>2</sub> redox flow cell. *J. Appl. Electrochem.* **2014**, *45*, 11–19. [[CrossRef](#)]
44. Suss, M.E.; Conforti, K.; Gilson, L.; Buie, C.R.; Bazant, M.Z. Membraneless flow battery leveraging flow-through heterogeneous porous media for improved power density and reduced crossover. *RSC Adv.* **2016**, *6*, 100209–100213. [[CrossRef](#)]
45. Hsieh, C.-T.; Teng, H.; Chen, W.-Y.; Cheng, Y.-S. Synthesis, characterization, and electrochemical capacitance of amino-functionalized carbon nanotube/carbon paper electrodes. *Carbon* **2010**, *48*, 4219–4229. [[CrossRef](#)]
46. Hsieh, C.-T.; Teng, H. Influence of oxygen treatment on electric double-layer capacitance of activated carbon fabrics. *Carbon* **2002**, *40*, 667–674. [[CrossRef](#)]